STATOR CURRENT SIGNAL CROSSING FOR FAULT DIAGNOSIS OF SELF-EXCITED INDUCTION GENERATORS

Fares Belynda[a,*], Radia Abdelli[a], Ahcene Bouzida[b]

[a] *Laboratoire de Technologie Industrielle et de l'Information LTII, Faculté de Technologie, Université de Bejaia, 06000 Bejaia, Algeria*

[b] *Faculty of Sciences and Applied Sciences, University Ali Mohand Oulhadj, 10000 Bouira, Algeria*

* corresponding author: belynda.fares@univ-bejaia.dz

ABSTRACT. This paper presents a novel method for modelling and diagnosis of electrical and mechanical faults in fixed-Speed Self-Excited Induction Generators (SEIGs) operating in autonomous mode in a small-scale wind energy system. The proposed method is validated using the finite element method. After the selection of the magnetising capacitors, the self-excitation process is performed under no-load conditions. Once the stator voltage is established, a symmetrical three-phase load is connected. The fault detection method introduced here is called Stator Current Signal Crossing (SCSC). The SCSC extracts a new signal from the stator currents, that enables the detection of stator inter turn short-circuits, broken rotor bars, and dynamic eccentricity faults in SEIGs. A spectral analysis of SCSC using the Fast Fourier Transform (FFT) algorithm is used to precisely locate the induced fault components. What sets this fault-tracking method apart from its predecessors is its exceptional ability to detect faults of any magnitude by analysing the modulation of the SCSC signal. These faults are directly identified by the presence of distinct harmonics, each indicative of a specific type of fault. This study also focuses on the SEIG in a wind energy system, whereas previous works have mainly addressed the induction machine in motor mode. In contrast, previous methods involved analysing a single current signal and isolating specific harmonics from a wide frequency range. The effectiveness of the proposed fault detection method and the self-excitation process are illustrated by simulation results and spectral analysis.

KEYWORDS: Self-Excited Induction Generator, wind energy, broken bars, inter-turn fault, dynamic eccentricity, FEM, diagnostic, Stator Currents Signal Crossing.

1. INTRODUCTION

Induction motors are used in many different types of industrial applications to convert electrical power into mechanical work. The main advantage of the induction machine is that it does not require a dedicated DC field excitation and has a robust brushless design. These machines are very efficient and reliable, and their power output can range from a few hundred watts to several megawatts.

Unlike their synchronous counterparts, induction machines have greater flexibility in how and at what speeds they can be operated. Induction machines are widely used as electrical generators in wind energy systems due to their low cost and high reliability. Wind turbines are used to power induction equipment using a gear box. The need for a gearbox arises from the need to convert the low rotor speeds generated by wind turbines to the high rotor speeds generated by electrical generators. Squirrel cage induction machines and wound rotor induction machines are the two main categories of induction machines based on the rotor design. Due to its reliability, low cost, and simplicity of design, the squirrel cage rotor design is widely used in off-grid wind power generation plants. Wind power generation systems that are connected to the power grid often choose wound rotor machines because of their high starting torque. The ability to extract rotor power without the added expense of power electronics in the rotor circuit is another advantage of massive rotors. This study focuses on the electricity generating part of a wind energy conversion system based on a Squirrel Cage Induction Generator (SCIG).

After introducing the SCIG, the electrical generator used in this work, with a brief description, the study proceeds to a comprehensive analysis of the SCIG operating in off-grid mode. The effect of magnetisation inductance on a SEIG is investigated. In addition to describing the effect of excitation capacitors, this paper also analyses the self-excitation process in a SCIG and presents its results.

The use of SEIGs in remote and rural wind energy systems shows the significance of closely monitoring their operation. The SEIG can have many problems, such as a broken rotor, shorted turns in the stator, rotor eccentricities, or an aging effect on the excitation capacitor. If the problem is not detected at an early stage, the whole system can completely break down. Broken rotor bars, shorted turns, and eccentricities can cause rotor asymmetry, unbalanced stator voltages, fluctuant torque, mechanical stress, thermal stress, and magnetic stress. Since wind turbines are

usually installed at remote sites on land or at sea, it is important to avoid expensive repairs and make sure the optimal amount of power is generated [1–3].

Literature classifies faults according to their location, development time, and nature; they may be sudden, intermittent, or progressive, depending on the speed of their occurrence and the duration of their development. It is difficult to discern between normal system variations and abnormal drift in operating conditions, making the identification of progressive problems a complex process. Several research studies have been carried out to investigate the external and internal faults of SEIG. In [4], due to the large peak currents in the stator windings, a sudden short-circuit at the terminals of an autonomous single-phase Self-Excited Induction Generator (SP-SEIG) could damage the generator. To avoid damage, only some experiments were performed for the case with one excitation capacitor in the auxiliary stator winding. In [5], a fast detection scheme based on the discrete wavelet transform (DWT) is used to analyse the transient behaviour of SEIG in the presence of a short circuit fault; the second generation wavelet transform (SGWT) is also used for fault detection. The processing time of SGWT is found to be shorter than that of DWT. An investigation into the use of a fault ride-through configuration in conjunction with a transient management scheme for the purpose of providing dynamic grid supports for SEIG-based wind turbines is explained [6]. To reduce oscillation and improve performance during and after faults, a new active damping control loop is created for the shunt compensation configuration. In reference [7], a new proposal is made to aid in the modelling and fault diagnosis of rotor and stator faults in an isolated wind energy conversion system. A generalised model of the squirrel-cage SEIG has been developed to simulate both the rotor and the stator faults, and an on-line fault diagnostic technique is implemented based on a spectral analysis of stator currents by the FFT algorithm. The combination of short-time Fourier transform and discrete wavelet transform algorithms is proposed as an additional contribution to the fault diagnosis of an SEIG. Using a generalised model to simulate the rotor and stator faults, an on-line fault diagnostic technique based on stator currents analysis of the SCIG is proposed for detecting stator and rotor failures [8].

In this study, the SEIG is modelled using the time-stepping finite element method (TSFEM) to analyse the self-excitation process and introduce the dynamic eccentricity, broken bars, and stator short circuit faults. Inspired by the Zero-Crossing-Time (ZCT) method used in many papers [9–11] and from the Three Phase Intersection Currents (TPIC) in [12], this work is based on the search for new signals for SEIG faults diagnosis. The ZCT technique involves collecting data for spectral analysis by monitoring the successive zero-crossing times of the current through the stator phases. The ZCT signal can be defined as

time difference between two consecutive points of the stator phase currents [9, 13, 14]. This paper presents a new approach to diagnosing the defects of SEIG by using an alternative to MCSA. This method for diagnosing SEIG faults uses a synthetic signal containing information about the timing and amplitude of three-phase current crossings.Because it is based on logical comparison operations, it is easy to implement and use online. The technique of the Stator Current Signal Crossing (SCSC) presents a simple and reliable improved method for SEIG fault diagnosis. Finding the positive and negative crossing points of the three-phase stator currents and then interpolating between them is how the SCSC is constructed. After that, a spectral analysis of this signal is carried out so that the fault signature can be extracted. The proposed method is first presented with a theoretical demonstration, and then validated using the finite elements method.

This detection technique is a new way of analysing complex electrical signals that include both current and voltage. It provides an alternative to the traditional method of analysing individual signals using the Fast Fourier Transform (FFT), as seen in previous research [15–17]. When analysing the current signal from a faulty SEIG experiencing using traditional methods, we encounter a problem. The signal becomes complicated, filled with numerous harmonics spread across the entire frequency range. This complexity makes it difficult to identify faults. Our proposed method considerably simplifies the analysis by highlighting fault indicators at basic frequencies, making it much easier to detect and understand faults. As a result, we don't need an exceptionally high sampling frequency for data collection, unlike traditional methods such as Motor Current Signature Analysis (MCSA), which require high sampling frequencies to track high-frequency harmonics.

2. AUTONOMOUS MODE OF SQUIRREL CAGE INDUCTION GENERATOR

In SEIG systems, it is important to provide the power needed to accelerate the induction machine above the synchronous speed. This is necessary to generate wind energy. When connected to an external source of reactive power, the SEIG can run and produce active power. Neither the prime mover nor the squirrel-cage rotor can produce the reactive power needed to generate the magnetic field. When a generator is connected to a grid and used with a bank of capacitors, the power factor value can be changed to provide some or all of the reactive power that is required [18, 19].

As the steady state operation of the SCIG under fault conditions is the main subject of this research, the investigation will focus on the operating point corresponding to the motor's rated current, which also determines the thermal derating limit.
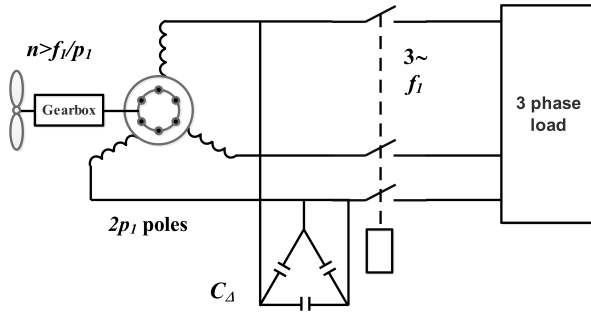
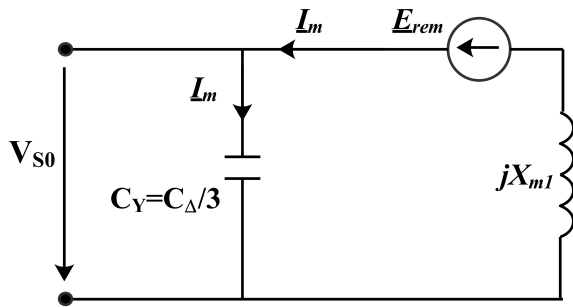FIGURE 1. SEIG in wind system with magnetization capacitor.

FIGURE 2. Ideal no-load SEIG per phase equivalent circuit.

FIGURE 3. Self-Excitation process of IG on no-load.
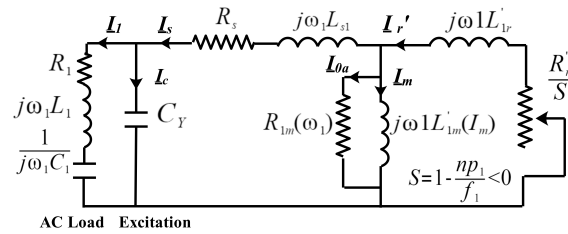
FIGURE 4. Self-Excited Induction Generator at load.

2.1. Squirrel cage induction generator self-excitation

To function as a generator, the squirrel cage induction machine must be driven at a speed greater than its no-load synchronous speed $\omega_1 = f_1/p_1$ and supplied with reactive power to generate and maintain its magnetic field. This reactive power can be generated by synchronous capacitors (Figure 1) [20].

The voltage V_s and frequency f_1 of the SEIG are primarily determined by machine parameters, capacitors C, and speed ω. The machine is driven by a fixed-speed wind turbine at speed n and still $\omega > f_1/p_1$. If there is any DC remanent magnetisation in the rotor, an AC emf is generated in the stator. Then, three-phase emfs at a frequency of $\omega_1 = f_1/p_1$ cause currents to flow in the stator phases and capacitors. Their phase angle is such that they create an airgap field that always increases the remanent field. This field then creates a higher stator emf, and so on, until the machine settles at a certain voltage V_s and frequency $f_1 \simeq p_1\omega$. If the speed is altered the frequency and the no-load voltage V_{s0} will also change (Figure 2).

By ignoring the machine's resistances and leakage reactances, a quasiquantitative study of this self-excitation process can be generated. The corresponding circuit degenerates to the circuit seen in Figure 2. The consequent modest emf E_{rem} ($E_{rem} = 2$ to $4\,\text{V}$) with the frequency $f_1 = p_1n$ indicates the presence of rotor remanent flux density (due to previous action).
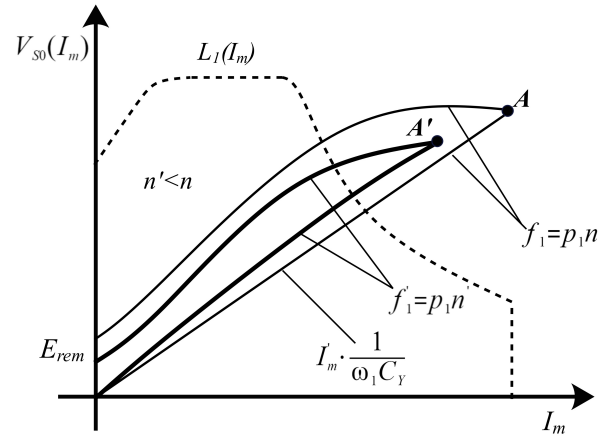
The frequency f_1 is primarily determined by speed. The machine Equation (1) becomes simple [21]:

$$V_{s0} = jX_{1m}I_m + E_{rem} = -j\frac{1}{\omega_1 C_Y}I_m = V_{s0}(\text{I}_m). \quad (1)$$

Simplifying the machine equation, the magnetisation characteristic $V_{s0}(I_m)$ is known to be nonlinear due to magnetic saturation, and it can be determined by the ideal no-load test at $f_1 = p_1n$. The voltage across a capacitor is proportional to its current. At no load, however, the current flowing through the capacitor is identical to the current flowing through the motor stator.

The schematic representation of Equation (1) can be seen in Figure 3.

In Figure 3, Opearting point A is the no-load voltage V_{s0} for speed, n, and C_Y. If the self-excitation takes place at a lower speed $n'(n' < n)$, a lower no-load voltage (point A'), V_{s0}', at a lower frequency $f_1' \sim p_1n'$ is obtained [21].

Figure 4 shows that the self-excitation process needs both the remanent magnetisation (E_{rem0}) and the magnetic saturation for it to work, that is, for the two curves to meet at a clear point.

When the magnetisation curve $V_{1m}(I_m)$ is known, we can use the complete equivalent circuit with a parallel capacitor CY over the terminals to examine the load characteristics.

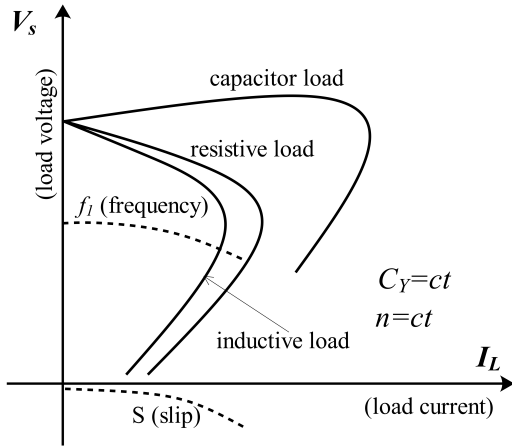For a given capacitor bank and rotation speed n, the load power factor affects the relationship between

FIGURE 5. Self-Excited Induction Generator load curves.

Parameter	Value
Rated power	400 kW
Rated voltage	400 V
Coupling	Delta
Poles Number	4
Speed	1597 (rpm)
Rated frequency	50 Hz

TABLE 1. SEIG parameters

FIGURE 6. Field distribution.

output voltage V_s and load current I_s (Figure 5).

As the load increases the slip also increases, and the frequency decreases. Consequently, the SEIG can generate power for a set of capacitors above a certain speed and magnetic saturation. Under load, both voltage and frequency drop significantly [21].

2.2. NUMERICAL SOLUTION OF SEIG USING FINITE ELEMENT METHOD

The development of robust numerical models of the SEIG that provide simulation of operation in conditions as close to reality as possible is necessary for the effective investigation of the complex characteristics of the SEIG. Circuit models and field-circuit models are two forms of numerical models that can be used for this purpose. Although SEIG circuit models are often simple to construct, they can give misleading results because they are based on simplistic assumptions that often ignore magnetic saturation, skin effect in rotor bars, tooth harmonics, etc.

The rapid advancement of computer hardware in recent years, particularly in terms of computing power and data storage, has opened up a new way of modelling and simulating operating states of electrical machines based on field-circuit models, which are typically 2D, unique models that can precisely account for specific phenomena. A complete model of an induction machine functioning as a motor or self-excited generator assumes a connection between the machine's finite element field model and the self-excitation circuit model. The field-circuit models are used to investigate the dynamic regimes of the SEIG under healthy and faulty operating conditions [4, 22].

In this paper, we perform a numerical solution for a 400 kW, 4 pole, self-excited squirrel cage induction generator (SEIG) producing 400 V rated voltage. For this study, the symmetry advantage cannot be used to reduce the domain for computing the 2D electromagnetic field due to the presence of asymmetrical,
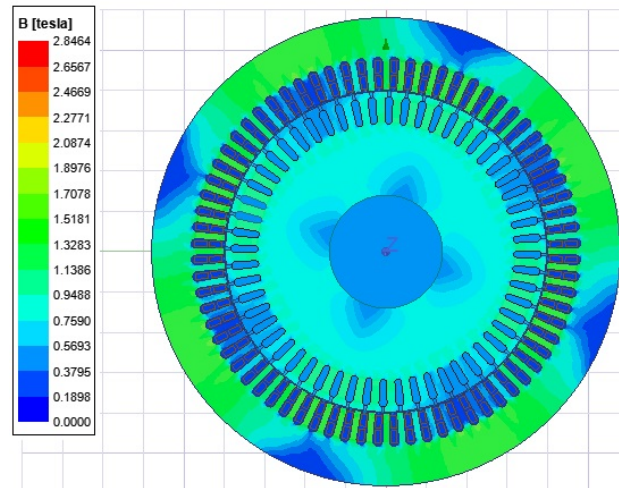
which are investigated in this paper.

The Self-Excited Induction Generator model is designed for healthy and faulty conditions using the time-stepping finite element method (TSFEM). The spatial distribution of the stator windings, the slots on both sides of the air gap, and the magnetic saturation of materials are all taken into account for the modeling of the SEIG. The Table 1 shows the SEIG parameters.

Reactive power is required for the induction machine to work as a standalone generator. The terminals of the armature windings are usually connected to a shunt capacitance bank to accomplish this task. The behaviour of this system has been extensively studied and the minimum capacitance value required to generate voltage has been calculated. This minimal value is often determined using the per phase equivalent technique. Therefore, for a given voltage, we obtain this capacitance by balancing the active and reactive powers [18, 19].

Figure 6 illustrates the field distribution in the machine's cross section when the stator voltage is established after the self-excitation phase.

The SEIG model is simulated with a 1597 rpm constant wind turbine speed and symmetric three-phase load conditions. As the initial conditions of SEIG, we use a very small stator current of 1 A to represent the initial magnetic flux required in the machine core to initiate voltage buildup. Without this current, SEIG voltage can not be produced.
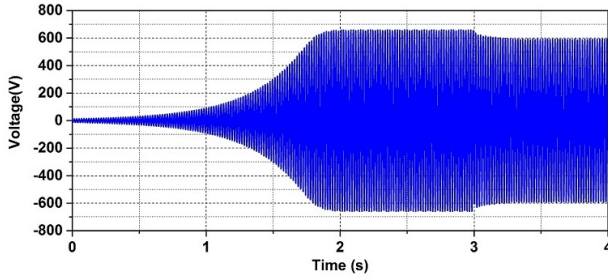
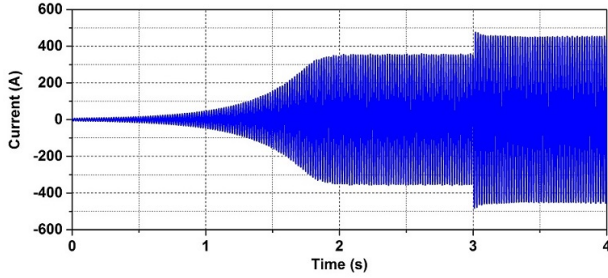FIGURE 7. SEIG buildup voltage during self-excitation process.

FIGURE 8. SEIG line current during self-excitation process.

FIGURE 9. SEIG electromagnetic torque during self-excitation process.

3. STATOR CURRENTS SIGNAL CROSSING FOR FAULT DETECTION

The developed model has also been tested and verified for use in dynamic operation during the self-starting of the SEIG. A no-load self-excitation of the generator is carried out from 0 s to 3 s and followed by a sudden connection of a three-phase balanced load to the stator. Using the stored data from the validated FEM model, Figures 7, 8, and 9 show the plots of the built-up stator voltage waveform, line current, and the electromagnetic torque present during the self-starting process when the rotor is driven at a fixed speed n.

The suggested detection method, based on Stator Currents Signal Crossing SCSC, is an alternative to motor current signature analysis (MCSA); the SCSC signal is generated by reconstructing the coordinates of the crossing points of the three-phase induced stator current waveforms of the SEIG.

This algorithm for finding points of intersection in polyphase signals uses complex and iterative calculations. This allows it find these intersections regardless of the polarity of the signal, and it can even handle situations with an infinite number of signals.

The algorithm employs advanced mathematical techniques, such as iterative methods, to precisely determine the precise instants at which these intersections occur. This capability to handle both positive and negative signals adds to its versatility, making it suitable for a wide range of applications in the field of signal processing.

Furthermore, its scalability to many signals makes a powerful tool for dealing with complex scenarios
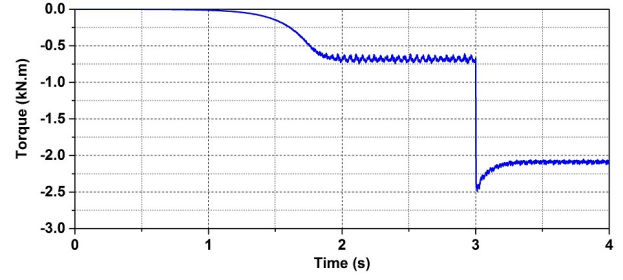
where multiple signals need to be analysed simultaneously. The ability of this algorithm to robustly and accurately detect intersections across such a wide spectrum of conditions underscores its significance in signal analysis and processing. The main steps of this procedure for the construction of the SCSC can be summarised as follows:

- For each sample $i(i = 1 : N)$, where N is the number of samples, a zero difference is sought between the current amplitude pairs $(I_a(i), I_b(i))$, $(I_a(i), I_c(i))$ of phases a, b, and c.

- The instants $t_a(i), t_b(i)$ and $t_c(i)$ are treated as the cross times.

- The amplitudes of the currents at the crossing times for sample i can be calculated by Equations (2), (3), and (4) as follows:

$$\begin{cases} t_{ab}(i) - t(i) \approx \varepsilon_t \\ I_{ab}(i) = I_a(i) \text{ if } I_a(i) - I_b(i) \approx \varepsilon_I \end{cases} \text{ for } (a, b), \quad (2)$$

$$\begin{cases} t_{ac}(i) - t(i) \approx \varepsilon_t \\ I_{ac}(i) = I_a(i) \text{ if } I_a(i) - I_c(i) \approx \varepsilon_I \end{cases} \text{ for } (a, c), \quad (3)$$

$$\begin{cases} t_{bc}(i) - t(i) \approx \varepsilon_t \\ I_{bc}(i) = I_b(i) \text{ if } I_b(i) - I_c(i) \approx \varepsilon_I \end{cases} \text{ for } (b, c). \quad (4)$$

However, a small error tolerance is used for the two successive samples i and $i + 1$ if the zero difference is not reached due to the sampling frequency. As a result, if the following criteria are met, we can identify a precise location where currents a, b, and c intersect:

$$\begin{cases} I_a(i) > I_b(i) \text{ and } I_a(i + 1) < I_b(i + 1) \\ or \\ I_a(i) < I_b(i) \text{ and } I_a(i + 1) > I_b(i + 1) \end{cases}, \quad (5)$$

$$\begin{cases} I_a(i) > I_c(i) \text{ and } I_a(i + 1) < I_c(i + 1) \\ or \\ I_a(i) < I_c(i) \text{ and } I_a(i + 1) > I_c(i + 1) \end{cases}, \quad (6)$$

$$\begin{cases} I_b(i) > I_c(i) \text{ and } I_b(i + 1) < I_c(i + 1) \\ or \\ I_b(i) < I_c(i) \text{ and } I_b(i + 1) > I_c(i + 1) \end{cases}. \quad (7)$$

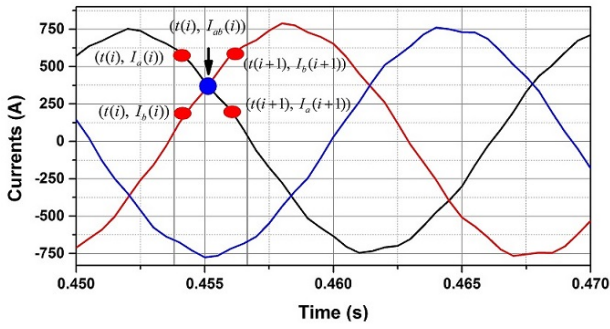To determine the coordinates of the crossing points, the stator currents I_j and I_k are linearly interpolated

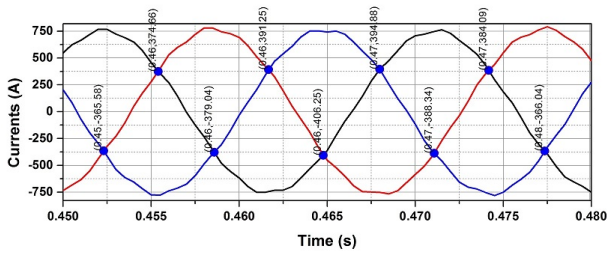Figure 10. Three-phase stator current crossing point localisation.

Figure 11. Three-phase stator current crossing points.

Figure 12. Positive side of SCSC (PSCSC).

Figure 13. Fully reconstructed SCSC.

between samples i and $i+1$, and the resulting line is represented by a line equation that is a function of the time and amplitude of the successive samples (Figure 10 and 11). This calculation's evolution produces Equations (8), (9), and (10) to determine the intersection time:

$$t_{ab}(i) = \frac{(I_b(i) - I_a(i)).t(i+1) - (I_b(i+1) - I_a(i+1)).t(i)}{(I_a(i+1) - I_a(i)) - (I_b(i+1) - I_b(i))}, \quad (8)$$

$$t_{ac}(i) = \frac{(I_c(i) - I_a(i)).t(i+1) - (I_c(i+1) - I_a(i+1)).t(i)}{(I_a(i+1) - I_a(i)) - (I_c(i+1) - I_c(i))}, \quad (9)$$

$$t_{bc}(i) = \frac{(I_c(i) - I_b(i)).t(i+1) - (I_c(i+1) - I_b(i+1)).t(i)}{(I_b(i+1) - I_b(i)) - (I_c(i+1) - I_c(i))}. \quad (10)$$

Similarly, the amplitude can be given by the Equations (11), (12), and (13) as:

$$I_{ab}(i) = \Delta I_a.t_{ab}(i) + \frac{I_a(i).t(i+1) - I_b(i+1).t(i)}{t(i+1) - t(i)}, \quad (11)$$

$$I_{ac}(i) = \Delta I_a.t_{ac}(i) + \frac{I_a(i).t(i+1) - I_c(i+1).t(i)}{t(i+1) - t(i)}, \quad (12)$$

$$I_{bc}(i) = \Delta I_a.t_{bc}(i) + \frac{I_b(i).t(i+1) - I_c(i+1).t(i)}{t(i+1) - t(i)}, \quad (13)$$

with ΔI_a being the slope of the line representing the current j between the two successive samples, and its expression is given by:

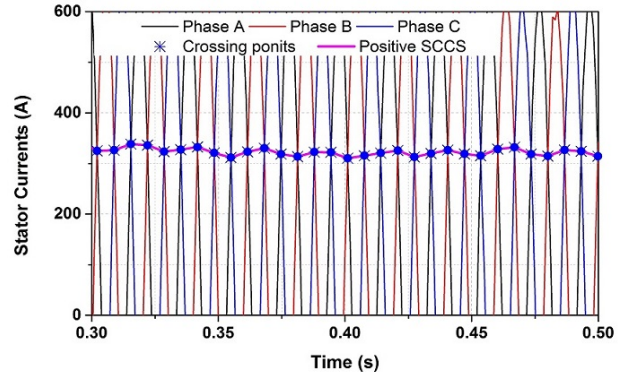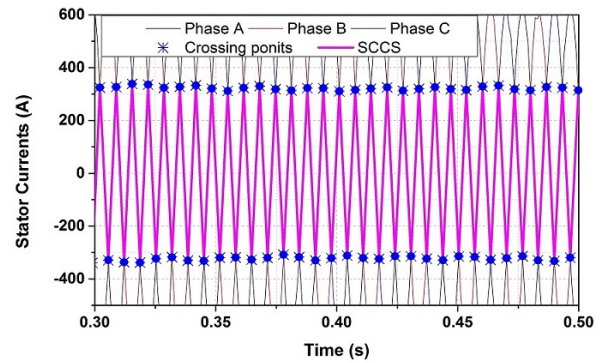$$\Delta I_a = \frac{I_a(i+1) - I_a(i)}{t(i+1) - t(i)}. \quad (14)$$

Using the time and amplitude of the three stator currents, the resulting crossing points are reconstructed in ascending time order for given 2 signals that can be used for the diagnostic machine. The positive side is called PSCSC and the fully reconstructed signal is called SCSC. They are shown in Figures 12 and 13 respectively.

In this case, the positive and negative cross signals have three intersections in one period of the stator currents, and their frequency will be $3f_s$. In Figure 14 the reconstructed waveform of the PSCSC for the SEIG under healthy and faulty conditions is shown.

3.1. Spectrum analysis of PSCSC and SCSC

The PSCSC and SCSC signals were reconstructed from the crossing points. The stator current samples were saved at a 2 kHz sampling frequency according to the simulation step of 0.0005 s, for an interval of 4 s in each simulation case. The PSCSC signal has three crossing points per period, giving period equal to $1/3f_s$ while the SCSC signal has six crossing points per period, giving a period equal to $1/6f_s$. The Fast Fourier Transform (FFT) was then applied to the PSCSC and SCSC signals in order to show their frequency spectrum for normal conditions. Based on the rotational speed, the stator current frequency, and the number of poles of the SEIG, we can get the fundamental frequency of the signals PSCSC and SCSC. Figures 15 and 16 show the frequency spectrums of
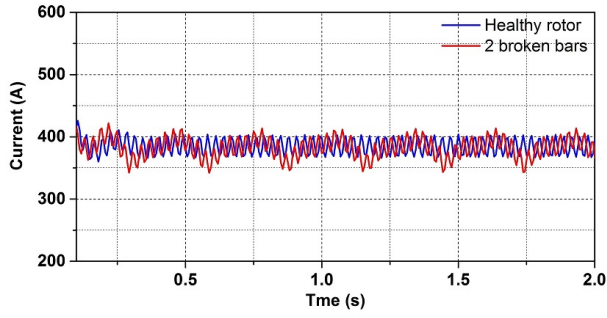
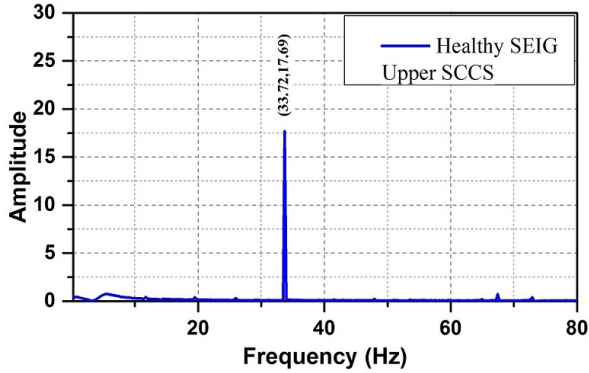FIGURE 14. PSCSC signal for a healthy and faulty SEIG.

FIGURE 15. Spectrum of PSCSC for healthy SEIG.

the SCSC and PSCSC. It can be seen that the positive and entire SCSC have a fundamental frequency f_{SCSC} and f_{PSCSC} located at 33.71 Hz and 126.04 Hz, respectively. The fundamental frequency of SCSC is only influenced by the speed of rotation, since its amplitude is influenced by the SEIG load level.

4. SEIG STATOR CURRENT MODULATION UNDER FAULTS

Recently, several demodulation techniques have been implemented. There are two basic classifications for these approaches: one-dimensional techniques and multi-dimensional techniques.

The first category requires the use of a single signal (such as a single stator current), whereas the second category requires the use of multiple signals, in this case, the three stator currents.

In addition to the peak detection method, one-dimensional methods include the synchronous demodulator, Hilbert transform, and Teager-Kaiser energy operator. There are two different types of multidimensional methods: direct and statistical methods. With regard to the first category, several techniques can be mentioned, such as the spatial vector, the park transform, the Concordia transform, and the study of symmetric components. Principal component analysis (PCA) and maximum likelihood estimation (MLE) are statistical approaches.
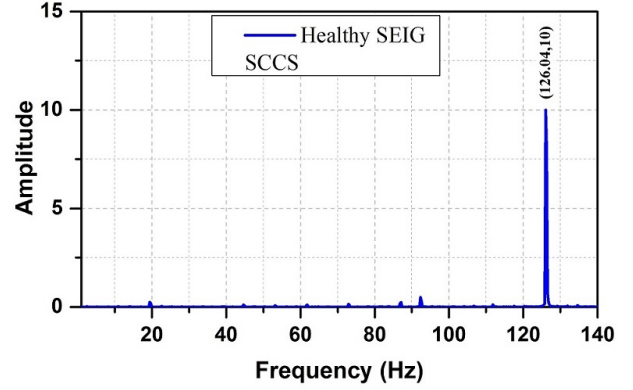

FIGURE 16. Spectrum of SCSC for healthy SEIG.

4.1. ROTOR BAR FAULTS

By modulating the stator's current when a motor is operating under normal conditions, the current generates a forward magnetic field that rotates at synchronous speed, which is defined as $s = 2f_s$. This field generates electromagnetic forces (EMFs) as it crosses the rotor, which causes a current to circulate in the rotor bars. The rotor continues to rotate until it reaches a speed that is ω_r greater than the synchronous speed on the Self-Excited Induction Generator. Concurrently, currents flowing through the rotor at a frequency $f_r = sf_s$ produce an additional forward magnetic field that rotates at the same synchronous speed as the stator.

When a rotor fault occurs, a backward magnetomotive force (MMF) will appear. This MMF will rotate at a speed of ω_s relative to the rotor, and it will rotate at speed of $(1-2s)f_s$ with relative the stator. As a direct result of this, an additional component in the stator current with a frequency of $(1-2s)f_s$ is introduced, and its expression is written in Equation (15) as follows:

$$I_{sf} = I_s \cos(\omega_s t) + I_L \cos((1-2s)\omega_s t), \qquad (15)$$

where I_{sf} is the resulting stator current under rotor broken bars.

The healthy motor has a stator current amplitude denoted by I_s, while the stator current component introduced by a rotor fault has an amplitude denoted by I_L. This lower sideband frequency component of $(1-2s)f_s$ can be used for diagnosing rotor faults. Furthermore, experimental evidence indicates the presence of an upper sideband component in the stator current spectrum with a frequency of $(1+2s)f_s$. These torque and speed oscillations occur at a frequency of $2ksf_s$ and are the result of the lower sideband component interacting with the stator field. A component of the stator current with a frequency of $(1+2s)f_s$ is generated by these oscillations [12].

4.2. DYNAMIC ECCENTRICITY MODULATION

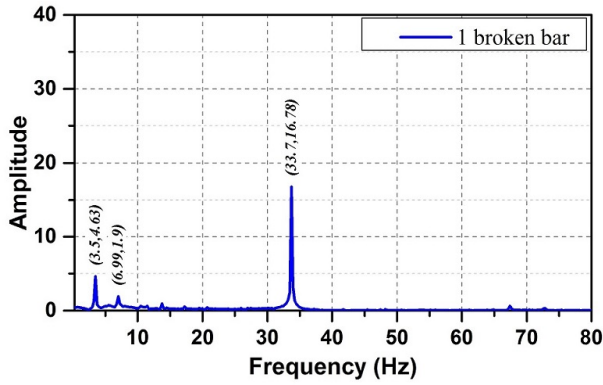When there is rotor eccentricity, the length of the airgap is no longer constant as a function of the sta-

FIGURE 17. Spectrum of PSCSC for SEIG with one broken bar.

FIGURE 18. Spectrum of PSCSC for SEIG with two broken bars.

FIGURE 19. Spectrum of PSCSC for SEIG with three broken bars.

tor circumferential angle and/or time. Equation (16) shows the modulation components of the dynamic eccentricity in the stator currents.

$$I_{DE} = \{I_s + (I_{de1} + I_{de2})\cos(\omega_r t)\}\cos(\omega_s t), \quad (16)$$

where I_{de1} and I_{de2} are the modulation amplitudes linked directly to the degree of dynamic eccentricity. Therefore, the eccentricity fault causes an amplitude modulation in the stator current with a frequency equal to f_{ecc}.

4.3. Short circuit modulation

One of the most common causes of electrical motor breakdowns is a short circuit in the stator windings, with the inter-turns short circuit being the most common. This type of failure causes an unbalanced electrical field, which leads to increased vibration in the motor and, resulting in deterioration of the insulation and failure of the bearings. When a short circuit occurs in the stator winding, an unbalanced distribution of the FMMs is present. FFT analysis of the stator current indicates the presence of a component at a frequency of $3.f_s$ [23, 24]. Since it is known that the frequency of the PSCSC signal is one third and the SCSC is one sixth of the frequency of the SEIG, the frequency f_s is used to identify the frequency of the short-circuit fault.

Due to the importance of detecting turn-to-turn shorts, a fault diagnostic approache using the amplitude of a reverse phase component (impedance) has also been investigated in recent works [23–25]. This was achieved by examining the FE circuit modeling. For fault identification, the majority of approaches use MCSA, vibration characteristics analysis, or a mix of both. Many of these proposed solutions use FFT to investigate at the spectrum to find the spectral characteristics.

5. Results and discussions

5.1. Broken rotor bars

The plots of the spectral analysis of the PSCSC obtained from SEIG with broken bars are shown in
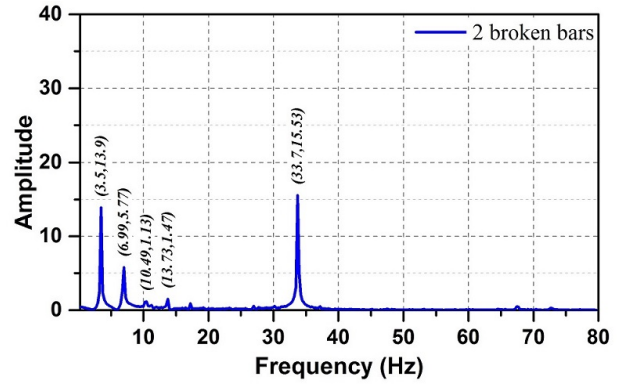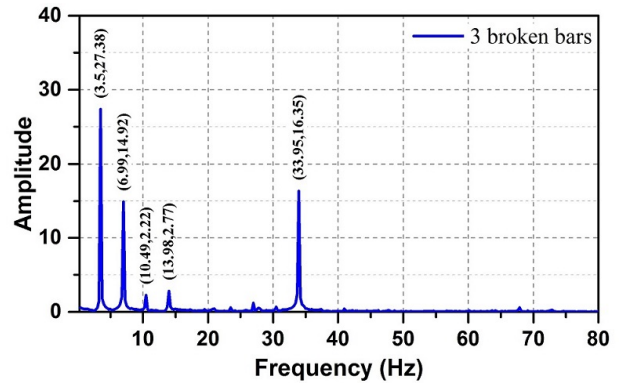
Figures 17, 18, and 19. The FFT plots show the presence of fixed components with a frequency equal to $2k.s.f_s$ (3.5 Hz, 6.99 Hz, 10.49 Hz, and 13.98 Hz) under the faulty conditions. These harmonics are clearly visible in the PSCSC spectrum as a result of a stator current amplitude modulation caused by a shift in the air gap's magnetic flux distribution. For this reason, the amplitude of these components can be measured and used as a means of identifying rotor cage failures.

The $2k.s.f_s$ amplitudes are not detected for the healthy operating conditions of the SEIG. The first component $2s.f_s$ is 4.63 A for one broken bar, 13.9 A for two broken bars, and 27.38 A for three broken bars. Therefore, the amplitude of the target component in the positive SCSC increases with the fault's intensity. In the case of SEIG with fixed load and speed operation conditions, the use of the SCSC method allows rotor bars diagnosis to detect the presence of these components. This result is an improvement over the traditional MCSA approach, where the fault diagnostic is difficult even when the SEIG has a single broken bar as the $(1 \pm 2s)f_s$ components are so close to the base frequency.

5.2. Inter-turns shrot-circuit

For the purpose of studying inter-turn short circuits in the SEIG, two faults were created in the stator winding as follows:
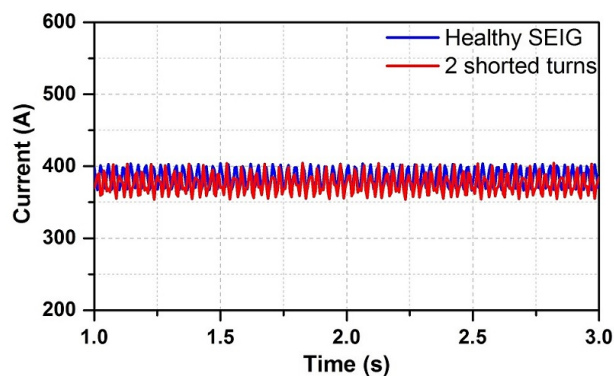
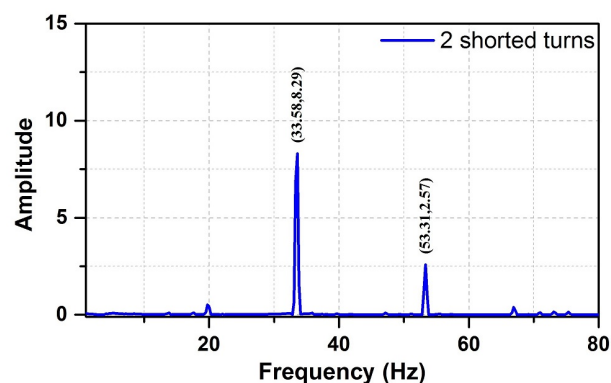FIGURE 20. PSCSC signal of SEIG with 2 shorted turns.

FIGURE 22. Spectrum of PSCSC for SEIG with 2 shorted coils.

FIGURE 21. Spectrum of PSCSC for SEIG with 2 shorted turns.
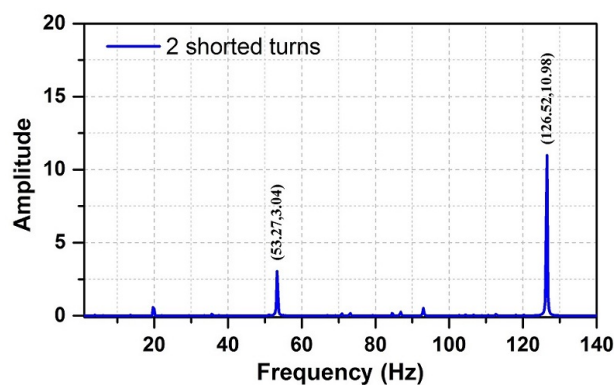
FIGURE 23. Spectrum of SCSC for SEIG with 2 shorted turns.

- A short-circuit between 2 turns of the same coil occurs in phase A.

- A short-circuit between 2 turns of adjacent coils occurs in phase A.

The simulation tests for inter-turn faults were performed on the studied SEIG. The stator windings inter-turn short-circuit is introduced in the developed external circuit linked to the FE model of SEIG. Figure 20 illustrates the effects of inter-turn faults on the PSCSC signal.

The FFT spectrums of the SCSC and PSCSC signals for inter-turn faults under operating conditions are shown in Figures 21, 22, 23, and 24. In this case, the sideband components are easily identifiable as they cluster closer to the fundamental frequencies f_{SCSC} and f_{PSCSC}.

The spectral analysis of PSCSC and SCSC shows the presence of a harmonic located at a frequency of 53.26 Hz close to the fundamental SCSC frequencies. A clear amplitude increase in the sideband f_s under loaded SEIG conditions ($s = -0.0652$) indicates the presence of an unbalanced distribution of FMM caused by shorted turns. The sensitivity of this distinctive component is increasing with the number of shorted turns of the stator. This sideband component cannot be clearly observed when analysing the line stator current, as the inte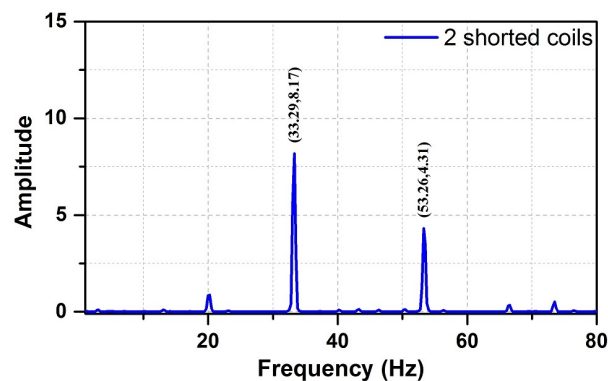r-turn fault detection is difficult at low load conditions. Identification of small FMM unbalanced distribution becomes practically possible with the SCSC analysis.

5.3. ROTOR ECCENTRICITY

The SEIG analysis model used for investigating the effects of dynamic eccentricity is shown in Figure 6. The Z-axis corresponds to the longitudinal direction of the stator and rotor core. The centre position of the axis is defined as $z = 0$ mm. In the case of dynamic eccentricity, the rotor position is shifted by the length e equal to 25 % and 50 % of the airgap length. The analyses are carried out under the same load condition with constant armature current. Figure 25 shows the positive SCSC obtained from healthy and 50 % eccentric SIEGs.

Using the above-mentioned PSCSC and SCSC signals, a spectral analysis study was carried out with a deliberately different SEIGS, in order to complement the validation of suitability of the proposed method for diagnosing dynamic eccentricity faults. Figures 26, 27, 28, and 29 show the spectrum of the PSCSC and SCSC obtained for the case of 25 % and 50 % eccentricity. As has been done for all the reconstructed PSCSC and SCSC, the DC level has been deliberately removed.

The obtained results are shown to be in good agreement with those obtained for healthy conditions. The
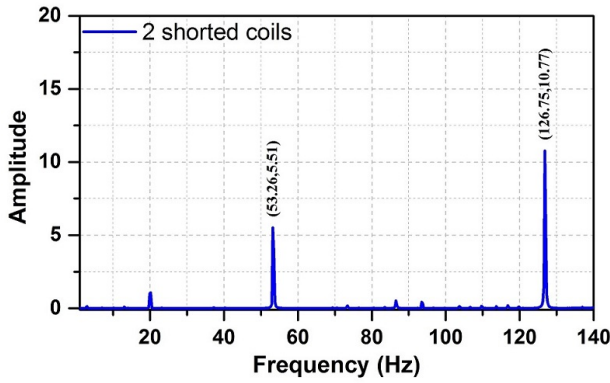
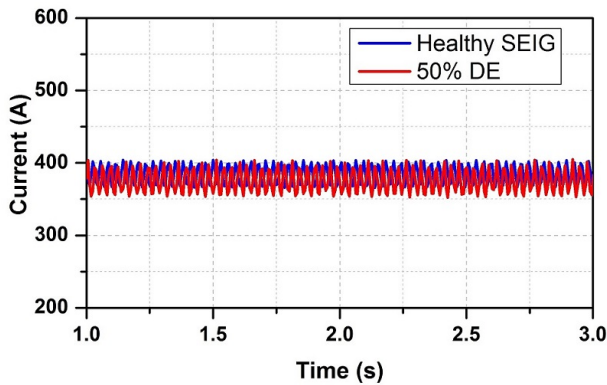FIGURE 24. Spectrum of SCSC for SEIG with 2 shorted coils.

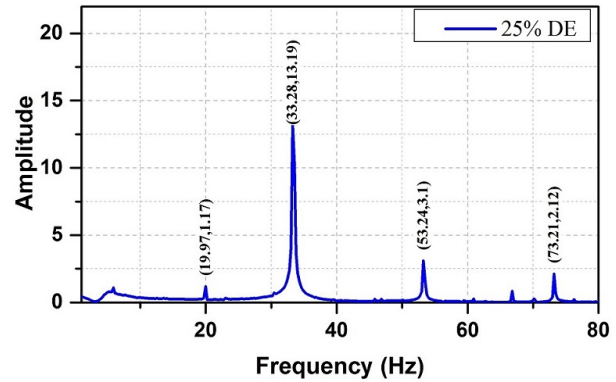FIGURE 25. Spectrum of SCSC for SEIG with 2 shorted coils.

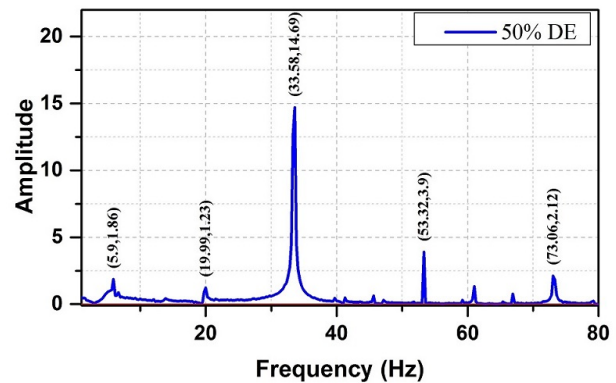FIGURE 26. Spectrum of PSCSC for SEIG with 25 % DE.

FIGURE 27. Spectrum of PSCSC for SEIG with 50 % DE.

spectrum obtained is characterised by the presence of new spectral components.

The FFT at the given load condition is as given in Figures 26, 27, 28, and 29, for the different SEIG eccentricity degrees. It is clearly observed that as the eccentricity increases, then the new harmonic amplitudes around the fundamental frequencies of the PSCSC and SCSC also increase. It is also observed that the dynamic eccentricity frequencies are unique for all the conditions, as can be observed for the 25 % and 50 % DE. Around the induced fault component of the PSCSC signal at frequency $f_{DE} = 53.26\,\mathrm{Hz}$, two symmetrical components are observed at $\pm 20\,\mathrm{Hz}$. The SCSC spectrum shows the presence of new symmetrical components located at frequencies $\pm 30\,\mathrm{Hz}$ around the central frequency of 53.26 Hz. Although the harmonics look good, the 25 % DE and 50 % DE increase the lower and upper side-band amplitudes of the central frequency.

It is very important to note that in a healthy SEIG, the spectra of the PSCSC and SCSC signals only show the fundamental ripple harmonics. There are no other signals that could interfere with the monitoring of specific harmonics that are associated with a fault. Otherwise, the only things that can change the amplitudes and frequencies of the fundamental harmonics of the PSCSC and SCSC signals are changes in the load level and the speed of rotation of the SEIG rotor. The appearance of new harmonics is therefore a clear and reliable indicator of the presence of an anomaly within the machine. This significant increase in harmonic content plays a key role in the early detection of anomalies, allowing timely corrective actions to be taken.

Finally, by comparing the spectra obtained for cases with and without faults, a clear and distinct appearance of harmonics indicative of faults is observed. Although eccentricities are among the most challenging faults to detect in electrical signal analysis, this method demonstrates that it is possible to identify these faults easily and quickly, regardless of their magnitudes. This advancement is critical to the early and accurate detection of electrical problems in SEIGs, thereby improving the reliability and safety of electrical systems.

6. CONCLUSION

The proposed Finite Element (FE) coupling-based numerical model of the fixed Speed Self-Excited Induction Generator for small autonomous isolated wind systems proved valuable in simulating the self-starting process and operation under load conditions. The simulation results showed that the SEIG generates a sinusoidal waveform, and the time required to reach
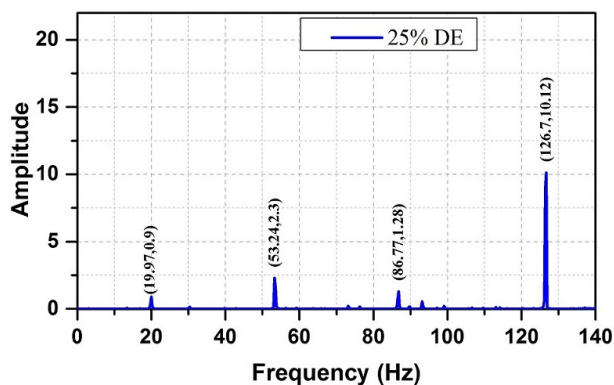
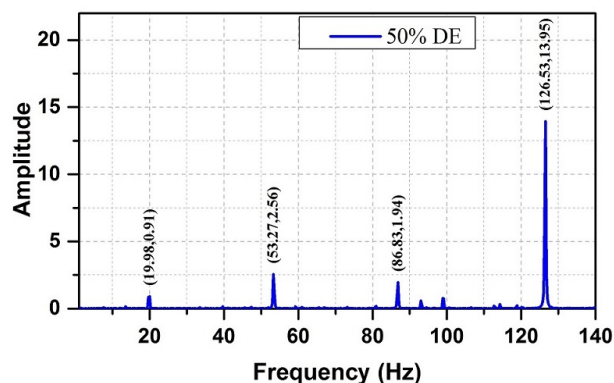FIGURE 28. Spectrum of SCSC for SEIG with 25 % DE.

FIGURE 29. Spectrum of SCSC for SEIG with 50 % DE.

a steady-state voltage varies depending on the capacitors used. In contrast, the FE model was used to investigate damaged rotor bars, inter-turn faults, and dynamic eccentricity. These faults were easily detected using the PSCSC and SCSC signals processed by spectral analysis. This novel approach to SEIG fault diagnosis is simple, effective, and has many advantages. It allows new signals to be reconstructed from three-phase stator currents, which contain the coordinates of the crossing points. The FFT is used to analyse this signal in the frequency domain, extracting the induced fault frequency components. The spectra reveal new frequencies associated with rotational frequency and sleep. These harmonics depend on the type of fault and, more importantly its severity. By examining the distinct harmonic patterns and their variations, it is possible not only to identify the specific fault, but also to assess its severity. This level of detail in spectral analysis provides a comprehensive understanding of the fault's characteristics, allowing for more accurate and effective diagnostic measures. It enables engineers and maintenance personnel to make informed decisions about the necessary repairs or maintenance, prioritising critical issues, and ensuring the reliability and longevity of SEIG systems. In the context of SEIG electrical or mechanical faults, spectrum analysis of PSCSC and SCSC is of great interest. This proposed solution is easy to implement and applicable to both offline and online monitoring systems.

References

[1] Y. M. Zamora, L. Hernández-Callejo, O. Duque-Pérez, V. Alonso-Gómez. Diagnosis of broken bars in wind turbine squirrel cage induction generator: Approach based on current signal and generative adversarial networks. *Applied Sciences* **11**(15):6942, 2021. `https://doi.org/10.3390/app11156942`

[2] M. Ojaghi, M. Sabouri, J. Faiz. Performance analysis of squirrel-cage induction motors under broken rotor bar and stator inter-turn fault conditions using analytical modeling. *IEEE Transactions on Magnetics* **54**(11):1–5, 2018. `https://doi.org/10.1109/tmag.2018.2842240`

[3] Y. K. Jelbaoui, E. M. Lamia, A. Saad. Fault diagnosis of a squirrel cage induction motor fed by an inverter using lissajous curve of an auxiliary winding voltage. *Indonesian Journal of Electrical Engineering and Computer Science* **21**(3):1299, 2021. `https://doi.org/10.11591/ijeecs.v21.i3.pp1299-1308`

[4] K. Makowski, A. Leicht. Behaviour of single-phase self-excited induction generator during short-circuit at terminals. *COMPEL - The international journal for computation and mathematics in electrical and electronic engineering* **37**(5):1815–1823, 2018. `https://doi.org/10.1108/compel-01-2018-0027`

[5] M. F. Khan, M. R. Khan, A. Iqbal. Modeling, implementation and analysis of a high (six) phase self excited induction generator. *Journal of Electrical Systems and Information Technology* **5**(3):794–812, 2018. `https://doi.org/10.1016/j.jesit.2016.12.016`

[6] P.-H. Huang, M. S. E. Moursi, W. Xiao, J. L. Kirtley. Fault ride-through configuration and transient management scheme for self-excited induction generator-based wind turbine. *IEEE Transactions on Sustainable Energy* **5**(1):148–159, 2014. `https://doi.org/10.1109/tste.2013.2277979`

[7] A. Ukil, S. Chen, A. Andenna. Detection of stator short circuit faults in three-phase induction motors using motor current zero crossing instants. *Electric Power Systems Research* **81**(4):1036–1044, 2011. `https://doi.org/10.1016/j.epsr.2010.12.003`

[8] I. Attoui, A. Omeiri. Modeling, control and fault diagnosis of an isolated wind energy conversion system with a self-excited induction generator subject to electrical faults. *Energy Conversion and Management* **82**:11–26, 2014. `https://doi.org/10.1016/j.enconman.2014.02.068`

[9] H. Çalış, A. Çakır. Experimental study for sensorless broken bar detection in induction motors. *Energy Conversion and Management* **49**(4):854–862, 2008. `https://doi.org/10.1016/j.enconman.2007.06.030`

[10] A. Çakır, H. Çalış, E. U. Küçüksille. Data mining approach for supply unbalance detection in induction motor. *Expert Systems with Applications* **36**(9):11808–11813, 2009. `https://doi.org/10.1016/j.eswa.2009.04.006`

[11] S. Haroun, A. N. Seghir, S. Touati. Multiple features extraction and selection for detection and classification of stator winding faults. *IET Electric Power Applications* **12**(3):339–346, 2017. `https://doi.org/10.1049/iet-epa.2017.0457`

[12] H. Khelfi, S. Hamdani. Induction motor rotor fault diagnosis using three-phase current intersection signal. *Electrical Engineering* **102**(2):539–548, 2019. https://doi.org/10.1007/s00202-019-00894-7

[13] A. Ukil, S. Chen, A. Andenna. Detection of stator short circuit faults in three-phase induction motors using motor current zero crossing instants. *Electric Power Systems Research* **81**(4):1036–1044, 2011. https://doi.org/10.1016/j.epsr.2010.12.003

[14] H. Çalış, A. Çakır. Rotor bar fault diagnosis in three phase induction motors by monitoring fluctuations of motor current zero crossing instants. *Electric Power Systems Research* **77**(5-6):385–392, 2007. https://doi.org/10.1016/j.epsr.2006.03.017

[15] I. Attoui, A. Omeiri. Modeling, control and fault diagnosis of an isolated wind energy conversion system with a self-excited induction generator subject to electrical faults. *Energy Conversion and Management* **82**:11–26, 2014. https://doi.org/10.1016/j.enconman.2014.02.068

[16] X. Gong, W. Qiao. Imbalance fault detection of direct-drive wind turbines using generator current signals. In *2013 IEEE Power and Energy Society General Meeting*. IEEE, 2013. https://doi.org/10.1109/pesmg.2013.6672920

[17] X. Gong, W. Qiao. Bearing fault diagnosis for direct-drive wind turbines via current-demodulated signals. *Industrial Electronics, IEEE Transactions on* **60**(8):3419–3428, 2013. https://doi.org/10.1109/tie.2013.2238871

[18] W. E. Vanco, F. B. Silva, F. A. S. Goncalves, C. A. Bissochi. Evaluation of the capacitor bank design for self-excitation in induction generators. *IEEE Latin America Transactions* **16**(2):482–488, 2018. https://doi.org/10.1109/tla.2018.8327403

[19] L. Wang, J.-D. Lee, S.-Y. Hu, et al. Design of three single-phase power-factor-correction boost converters joined with a controllable singe-phase inverter for a self-excited induction generator. In *2019 IEEE Industry Applications Society Annual Meeting*, pp. 1–9. IEEE, 2019. https://doi.org/10.1109/ias.2019.8912324

[20] V. Chenchevoi, I. Zachepa, O. Chencheva, R. Yatsiuk. Parameters of guaranteed self-excitation of an induction generator for autonomous electric power sources. In *2020 IEEE Problems of Automated Electrodrive. Theory and Practice (PAEP)*, pp. 1–4. IEEE, 2020. https://doi.org/10.1109/paep49887.2020.9240851

[21] I. Boldea, S. A. Nasar. *The Induction Machines Design Handbook*. CRC Press, 2018. https://doi.org/10.1201/9781315222592

[22] B. Rezaeealam. Calculation of magnetizing and leakage inductances of induction machine using finite element method. *Electrical Engineering* **103**(1):315–323, 2020. https://doi.org/10.1007/s00202-020-01082-8

[23] A. Zorig, S. H. Kia, A. Chouder, A. Rabhi. A comparative study for stator winding inter-turn short-circuit fault detection based on harmonic analysis of induction machine signatures. *Mathematics and Computers in Simulation* **196**:273–288, 2022. https://doi.org/10.1016/j.matcom.2022.01.019

[24] X. Liang, M. Z. Ali, H. Zhang. Induction motors fault diagnosis using finite element method: A review. *IEEE Transactions on Industry Applications* **56**(2):1205–1217, 2020. https://doi.org/10.1109/tia.2019.2958908

[25] A. Zorig, S. H. Kia, A. Chouder, A. Rabhi. A comparative study for stator winding inter-turn short-circuit fault detection based on harmonic analysis of induction machine signatures. *Mathematics and Computers in Simulation* **196**:273–288, 2022. https://doi.org/10.1016/j.matcom.2022.01.019